Heliyon 10 (2024) e34823

Contents lists available at ScienceDirect

Heliyon

journal homepage: www.cell.com/heliyon

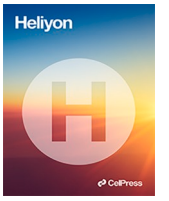

Research article

Mechanism of Yishen Chuchan decoction intervention of Parkinson's disease based on network pharmacology and experimental verification

Dong Di [b,c,1], Chencheng Zhang [d,1], Suping Sun [b,c], Ke Pei [b], Renjun Gu [b], Yan Sun [b,c], Shihan Zhou [b,c], Yanqing Wang [b,c], Xinyi Chen [b,c], Shan Jiang [a], Haoxin Wu [b,c], Boran Zhu [b,c,*], Xu Xu [a,b,**]

[a] *Nantong TCM Hospital Affiliated to Nanjing University of Chinese Medicine, Nantong, Jiangsu, 226001, China*
[b] *Nanjing University of Chinese Medicine, Nanjing, 210023, Jiangsu, China*
[c] *Key Laboratory of Integrative Biomedicine for Brain Diseases, College of Traditional Chinese Medicine, Nanjing University of Chinese Medicine, Nanjing, Jiangsu, 210046, China*
[d] *Institute of Oncology, Affiliated Tumor Hospital of Nantong University, Nantong, 226631, Jiangsu, China*

A R T I C L E I N F O

Keywords:
Parkinson's disease
p38 MAPK
Medicated serum
Traditional Chinese medicine
Network pharmacology
Rotenone

A B S T R A C T

The incidence of Parkinson's disease (PD) rises rapidly with the increase of age. With the advent of global aging, the number of patients with PD is rising along with the elderly population, especially in China. Previously, we found that Yishen chuchan decoction (YCD), prescribed based on clinical experience, has the potential of alleviating symptoms, delaying the progression, and controlling the development of PD. Nonetheless, the underlying mechanistic role is yet to be explored.

Aim: This research examined the possible therapeutic effects of YCD in alleviating PD *via* a systematic approach with network pharmacology and experimental validation, aiming at providing a new understanding of traditional Chinese medicine management regarding PD.

Methods: The chemical structure and properties of YCD were adopted from Traditional Chinese Medicine System Pharmacology Database (TCMSP), SwissADME, PubChem, and PubMed. The potential targets for YCD and PD were identified using Swiss Target Prediction, GeneCard, PubChem, and UniProt. The herbal-component-target network was created *via* the Cytoscape software. Moreover, by using the STRING database, the protein-protein interaction (PPI) network was screened. Gene function GO and KEGG pathway enrichment analyses were performed *via* the Metascape database. YCD-medicated Rat Serum from Sprague-Dawley (SD) Rats was prepared, and SH-SY5Y cells were preconditioned with rotenone to develop the PD model. To examine the impact of YCD on these cells and explore the mechanistic role of the p38 mitogen-activated protein kinase (MAPK) pathway, the cells were pretreated with either serum or a p38 MAPK pathway inhibitor. This study employed the Cell Counting Kit (CCK)-8 assay and Hoechst 33,342 staining to evaluate the viability and morphological changes induced by the YCD-medicated rat serum on rotenone-treated SH-SY5Y cells. Apoptosis was assessed by Flow cytometry.

* Corresponding author. Key Laboratory of Integrative Biomedicine for Brain Diseases, College of Traditional Chinese Medicine, Nanjing University of Chinese Medicine, Nanjing, Jiangsu, China.
** Corresponding author. Nantong TCM Hospital Affiliated to Nanjing University of Chinese Medicine, Nantong, Jiangsu, China.
E-mail addresses: zhuboran@njucm.edu.cn (B. Zhu), 15606296788@163.com (X. Xu).
[1] Dong Di and Chencheng Zhang contributed equally to this work.

https://doi.org/10.1016/j.heliyon.2024.e34823
Received 17 October 2023; Received in revised form 16 July 2024; Accepted 17 July 2024
Available online 18 July 2024

Immunofluorescence staining assessed the microtubule-associated protein 2 (MAP2) level. Enzyme-linked immunosorbent assay (ELISA) was employed to quantify the concentrations of inflammatory mediators interleukin-1β (IL-1β), interleukin-6 (IL-6) and tumor necrosis factor-alpha (TNF-α). Also, reactive oxygen species (ROS) and superoxide dismutase (SOD) levels were determined. Western Blotting measured the expression of total and phospho-p38 MAPK (p-p38).

Results: This study identified 65 active components in YCD, which were found to target 801 specific genes. By screening, 63 potential core targets were identified from a pool of 172 overlapping targets between PD and YCD. These targets were examined by GO and KEGG analyses revealing their substantial correlation to MAPK, PI3K-Akt signaling pathways, positively controlling protein phosphorylation, and pathways of neurodegenerative diseases. SH-SY5Y cells were treated with 2 μM rotenone for 48 h, which reduced cell viability to 50 %, and reduced MAP2 expression, increased the rate of apoptosis, oxidative stress, inflammation, and p-p38 expressions. YCD-medicated rat serum significantly improved the viability, reduced the apoptosis rate, and increased the MAP2 expression. YCD-medicated serum increased SOD, reduced ROS and suppressed IL-6, IL-1β and TNF-α levels, thus inhibiting oxidative stress and inflammation in rotenone-treated SH-SY5Y cells. Moreover, YCD-medicated serum substantially lowered the p-p38 expression induced by rotenone. SB203580, a specific inhibitor of p38 MAPK, could also inhibit the p-p38 expression, apoptosis, and restore morphological damage of cells, also improve inflammation and oxidative stress.

Conclusion: YCD enhanced cell viability and reduced apoptosis rate, inflammation, and oxidative stress in vitro. These beneficial effects could potentially involve the suppression of p38 pathway and suppressed the phosphorylation of p38 MAPK.

1. Introduction

PD is a commonly known neurodegenerative condition that predominantly affects the elderly population. It is characterized by abnormal accumulation of α-synuclein (α-syn) and degeneration of dopaminergic (DA) neurons within the substantia nigra pars compacta (SNc) area in the midbrain, its main manifestations are static tremor, bradykinesia, rigidity, and non-motor symptoms [1–3]. The population-wide prevalence of PD is about 0.3 %, doubling with age, reaching 4 % at age 85 [4]. Levodopa and various drugs with neuronal protective effects, such as monoamine oxidase B (MAO-B) inhibitors, dopamine receptor (DR) agonists, and anticholinergics [5], can be used as treatment options for PD under specific conditions. However, these treatment options have many contraindications and toxic side effects, also constituting an economic burden at individual and global levels.

Currently, it is vital to explore a new therapeutic method to delay the progression of PD when prodromal symptoms appear [6,7]. Over the past few decades, Traditional Chinese Medicine (TCM) has gained wider acceptance among the public and the medical community as it has been effective in dealing with a variety of conditions in many countries. TCM possesses multiple notable advantages of its component targets and pathways. Clinical studies have shown that TCM compounds, extracts and prescriptions can improve motor and non-motor symptoms, reduce the dose of dopaminergic drugs and the occurrence of motor disorders. The

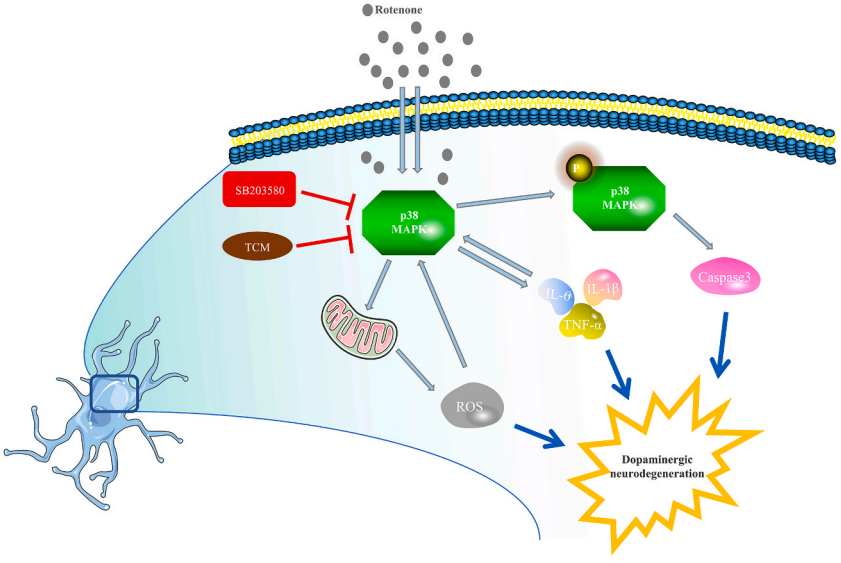

Fig. 1. P38 MAPK is involved in neuroinflammation and cell damage in rotenone-treated PD progression.

underlying processes and clinical reliability in treating PD can be verified *via* network pharmacology. Liu et al. used the network pharmacology (NP) and molecular docking approach to examine the possible mechanistic role of Suanzaoren decoction in treating PD with sleep disorders [8]. Zhuang et al. demonstrated that polyphenols from *Toona sinensis* seeds could improve the neuroinflammation of 6-hydroxydopamine (6-OHDA)-treated PC12 as well as rat model of PD by inhibiting the p38 MAPK signaling pathway [9]. Many reports have confirmed that Qian-Zheng San and Da-Bu-Yin-Wan can improve the behavioral impairment of mice model of PD and improve the morphological structure of neuronal mitochondria by regulating the expression of mitochondrial genes [10,11]. In conclusion, exploring the compounds and extracts of Chinese herbal medicine has a good prospect in developing new drugs for PD [12].

YCD is a clinical experience-based treatment modality for PD, which is composed of R*adix astragali*, *Fructus gardeniae*, *Herba cistanches*, *Radix rehmanniae*, *Radix aconiti preparata* and *Radix aconiti kusnezoffii preparata*. In this study, through network pharmacology and experimental verification, we matched compound targets of YCD with PD-related targets, screened out corresponding therapeutic pathways, and chose the highly consistent pathway to verify.

He et al. [13] summarized previous papers showing that neuroinflammation in patients with PD is an important pathological factor. Proinflammatory substances such as Rotenone and 1-methyl-4-phenyl-1,2,3,6-tetrahydropyridine (MPTP) activate microglial cells, and induce the release of *IL-6, IL-1β*, and *TNF-α* leading to DA neuron degeneration and damage. Proinflammatory substances also activate the p38 MAPK in the substantia nigra, leading to up-regulation of p-p38, further mediating the up-regulation of cyclooxygenase-2 (COX-2) and activation of caspase-3, also resulting in DA neurons degeneration (Fig. 1). Our research attempted to validate the p38 MAPK pathway involvement in the potential therapeutic effect of YCD in PD. Our study explored a novel pathway for the prevention and treatment of PD using TCM.

2. Materials and methods

2.1. Network pharmacology

The schematic illustration of NP research methods is depicted in Fig. 2.

2.1.1. Herbal-compound-target network construction of the YCD

The chemical compositions of each herbal component were screened *via* TCMSP (https://old.tcmsp-e.com/tcmsp.php) [14], as well as research published in PubMed. The selection of compounds was depending on their oral bioavailability (OB) ≥ 30 % [15] and drug-likeness (DL) ≥ 0.18 [16]. PubChem (https://pubchem.ncbi.nlm.nih.gov) acquired 3D sdf and molecular structure for each herbal component. Subsequently, the obtained 3Dsdf file was deposited to the platform of SwissADME (http://www.swissadme.ch) [17] to assess pharmacokinetic properties and drug similarity. Also, the molecular structure was deposited into the platform of Swiss

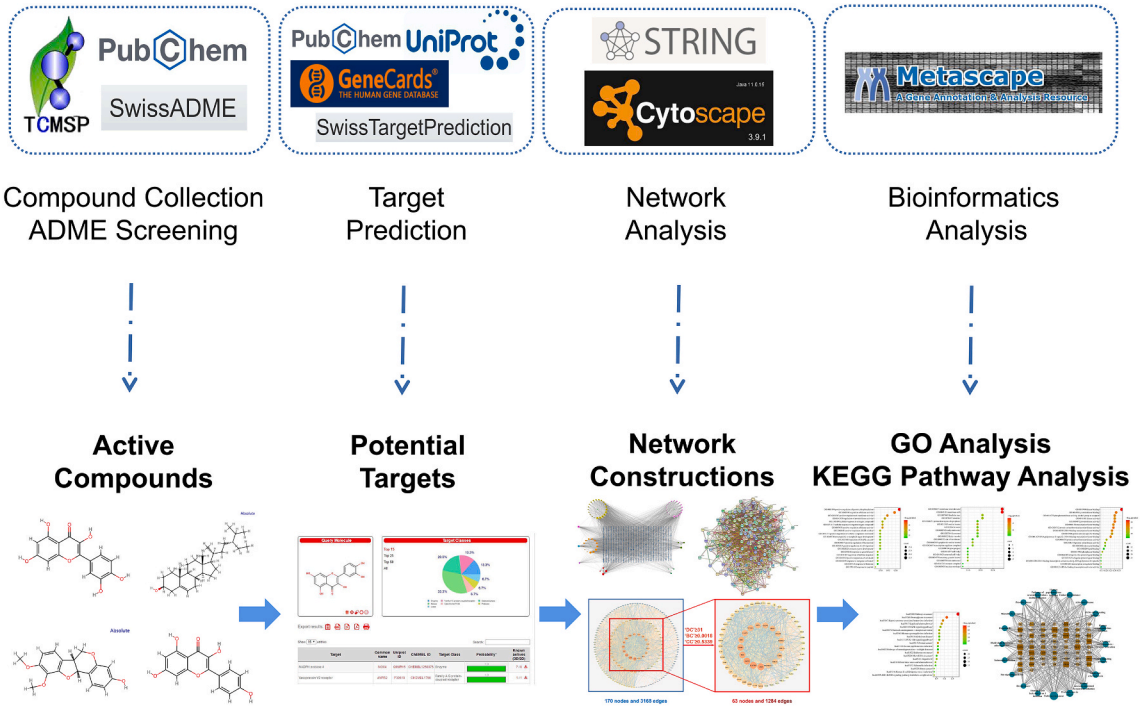

Fig. 2. A framework of research methodology based on NP.

Target Prediction (http://www.swisstargetprediction.ch) [18] to predict the potential targets. These potential targets were consolidated into the Uniprot protein database (https://www.uniprot.org) to verify their accuracy and perform protein-gene docking. Subsequently, the herbs and their corresponding components and possible targets were uploaded into the software of Cytoscape 3.7.2s [19] to establish the network of interconnections within the herb, its components, and targets. Degree value quantifies the connectivity of a particular target, whereby a higher degree value indicates a greater number of associations.

2.1.2. PPI network construction and potential core targets selection

GeneCards (https://www.genecards.org) [20] platform was utilized to obtain PD targeted genes by using the keyword "Parkinson's disease." Genes with scores exceeding the median degree were chosen for further analysis. The identified YCD and PD-related targets were entered into Bioinformatics (http://www.bioinformatics.com.cn) to obtain the genes that intersect the herbal components and PD. The intersection genes were uploaded to the STRING (https://string-db.org) platform to screen and generate the PPI network. Cytoscape 3.7.2 software was utilized to screen potential core targets and construct a creening strategy diagram based on the comprehensive ranking of node degree centrality (DC), node closeness centrality (CC), and node betweenness centrality (BC).

2.1.3. GO and KEGG enrichment analysis

Metascape (http://metascape.org) platform was employed to upload the core targets for GO and KEGG enrichment analysis. The outcomes were visualized *via* the Bioinformatics platform, and KEGG outcomes were uploaded into the software Cytoscape 3.7.2 to create the "core target-critical pathway" network.

2.2. Herbal extracts preparation

YCD comprised six distinct herbal extracts. The detailed composition of YCD is displayed in Table S1. These herbs were procured from the TCM Pharmacy of the Jiangsu Hospital of TCM. To ensure their authenticity, the herbal extracts were tested with rigorous authentication procedures. Voucher specimens, identified by the voucher number NZY-ZHU-20221211, were duly archived in the Herbarium of the Laboratory of Encephalopathy at Nanjing University of Chinese Medicine. *R. astragali* ($60 \pm 2\times g$), *F. gardeniae* (10 ± 1 g), *H. cistanches* (15 ± 1 g), *R. rehmanniae* (20 ± 1 g), *R. aconiti preparata* (20 ± 1 g), and *R. aconiti kusnezoffii preparata* (20 ± 1 g) were soaked in 2 L of dH2O for 1 h. After boiling for 1 h, the resulting mixture was subsequently filtrated *via* a double layer of gauze. The residual material was further boiled for 30 min with 1 L of dH2O. The obtained filtrates were combined and concentrated, resulting in a 400 mL mixing solution. The mixture was concentrated at 0.5 g/mL and 1 g/mL (net content). The YCD potion was ultimately kept at −20 °C. The quality of various YCD batches was assessed using the Waters 2695 Alliance HPLC system (Waters Corp, Milford, MA, U.S.A.). The mobile phase comprised a 0.1 % aqueous solution of phosphoric acid (A) and acetonitrile (B). The flow rate was set at 1 mL/min along with 210 nm detection wavelength. The mobile gradient phase consisted of specific time intervals, from 0-10 min to 2–8% B; 10–45 min, 8–28 % B; 45–50 min, 28–40 % B; 50–55 min, 40–95 % B; 55–63 min, 95-2% B, representing the sample elution. During experimentation, the oven was set at 30 °C. This study employed a chromatographic column composed of Apollo C18 (Kromasil, 100-5-C18, 46 mm × 250 mm, 5 μm). The YCD profile is depicted in Fig. S1.

2.3. Reagents and antibodies

All antibodies and chemical compounds were procured as follows: Rabbit anti-P38 MAPK and rabbit anti-phospho-p38 MAPK from Affinity Biosciences (Jiangsu, China). Mouse anti-β-tubulin, Horseradish peroxidase (HRP)-Labeled goat anti-rabbit IgG and goat anti-mouse IgG from ZSGB-BIO (Beijing, China). Rotenone and Mouse anti-MAP2 antibodies from Sigma-Aldrich (Merck KGaA, Darmstadt, Germany). Fluorescein isothiocyanate (FITC)-labeled goat anti-mouse IgG antibodies from Abcam (Cambridge, MA, USA).

2.4. Animals

This study comprised twenty SD rats, with ten males and ten females aged 7–8 weeks, from Jiangsu Huasino Pharmaceutical Technology Co., Ltd (Jiangsu, China). The rats were confirmed to be free from any pathogenic environment and were allowed to be raised in accordance with established protocols, under standard laboratory conditions 18–22 °C, with relative humidity at 50–60 %, along with 12 h: 12 h of the light & dark cycle. Rats were given a standard laboratory diet with free access to food and water. All experiments strictly adhered to the institutional animal care guidelines (202106A024) suggested by the Experimental Animal Ethics Committee of Nanjing University of Chinese Medicine.

2.5. Medicated serum preparation

400 mL of the mixed filtrate prepared in step 2.2. was concentrated to 200 mL. The rats were categorized into two groups, each group had half male and half female. One group was given YCD intragastric administration with the dose of 9 mL/kg (according to the concentration of YCD decoction and rat's surface area [21,22]), and the other group was given the same proportion of normal saline (NS) for 7 days, once in the morning and once in the evening. After 1 h of the last administration, the rat's blood was withdrawn from the abdominal aorta under pentobarbital anesthesia. The separated serum was centrifuged for 10 min at 3000 rpm, heat-inactivated for 30 min (55 °C), followed by filtration (0.22 μm), and kept at −80 °C.

2.6. Culture and treatment of SH-SY5Y cell line

SH-SY5Y cells were obtained from the Shanghai Cell Bank (Chinese Academy of Sciences) and grown in culture flasks using Dulbecco's Modified Eagle's Medium enriched with 10 % fetal bovine serum (Gibco, Grand Island, NY, USA) and 1 % Penicillin-Streptomycin (Hyclone, South Logan, UT, USA). The cells were maintained in a humidified cell culture condition (5 % CO2) (37 °C). The culture medium was refreshed on alternate days, while cell passaging was performed every 3–4 days at 2×10^5 cells/mL. Following passage for 3 times, cells with good growth state and density of 50–60 % were selected for subsequent experiments.

PD cell model was developed by treating SH-SY5Y cells with various concentrations (1, 2, 4, and 6 μM) of rotenone for respective time intervals, 0, 6, 12, 24, and 48 h. The modeling conditions were determined based on the concentration and duration of rotenone intervention required to achieve 50 % cell activity. Various concentrations (0, 5, 10, and 20 %) of YCD-medicated serum or 10 μM(final concentration) of the p38 MAPK pathway selective inhibitor SB203580 was introduced prior to the application of rotenone.

2.7. Cell counting kit-8 assay

Cells under the logarithmic growth phase were converted into a single-cell suspension, which was subsequently seeded into a cell culture plate at 1×10^5 cells/well (96 wells). Following 24 h, the cells exhibited a notable capacity for adherence and a fast growth rate. The cells were pretreated with various concentrations of Rotenone, YCD-medicated serum and Non-medicated serum, and subsequently washed with PBS. Then cells were incubated with CCK-8 (10 μL) (CK04, dojindo, Shanghai, China) for 3 h at 37 °C. Each well's optical density (OD) was measured at 450 nm using a microplate reader.

2.8. Immunofluorescence staining

Cells were grown in a confocal dish, and the Rotenone, SB203580, YCD-medicated serum and Non-medicated serum treatments were administered once the cell density reached 50–60 %. The drug medium was discarded post-treatment and subsequently washed. These cells were fixed for 15 min *via* paraformaldehyde (4 %), followed by washing. Subsequently, cell specimens were permeated using a 1 % Triton solution for 10 min, followed by blocking with a 4 % BSA for 1 h. Following the blocking, cells were incubated with mouse anti-MAP2 (1:500, M1406, Sigma-Aldrich) antibodies for 12–16 h (4 °C). Subsequently, the cells were placed in the dark with FITC-labeled goat anti-mouse IgG (ab150115, Abcam) antibodies for 1 h at room temperature. Next, the cells were washed and placed in a confocal laser scanning microscope (SP5; Leica, Wetzlar, Germany) for visual examination. The data was processed *via* Leica Application Suite X (LAS X) software (SP5; Leica, Wetzlar, Germany).

2.9. Hoechst 33,342 staining

Approximately 1×10^6 cells/well were cultured in a culture well plate (12 wells) and treated once the cell density reached 50–60 %. Subsequently, cells were stained with 500 μL of Hoechst 33,342 (C1025, Beyotime, Shanghai, China) for 20 min (37 °C). After washing, the cells were visualized using a fluorescence microscope (FV1000, Olympus Optical Co., Ltd, Tokyo, Japan). ImageJ (National Institutes of Health, Maryland, USA) software was used to analyse the size of the nucleus.

2.10. Enzyme-linked immunosorbent assay

The intracellular levels of *IL-1β*, *IL-6,* and *TNF-α* were quantified using ELISA kits (R&D systems, Minneapolis, MN, United States).

2.11. Oxidative stress analysis

ROS level was measured *via* ROS/Superoxide kit (S0033S, Beyotime). The SOD activity was monitored *via* SOD kit (S0101S, Beyotime).

2.12. Flow cytometry

Cells were trypsinized, then washed in PBS. Afterward, the cells were tagged with annexin V-fluorescein isothiocyanate (V-FITC) and propidium iodide (PI) (C1062L, Beyotime). The flow cytometer (Gallios, Beckman Coulter Inc, CA, United States) was employed to examine the cell apoptotic rate. The apoptotic cells were categorized into four distinct quadrants: Q4, early apoptotic cells; Q2, late apoptotic cells; Q3, live cells, and Q1, dead cells. The apoptosis rate was determined *via* formula: apoptotic rate = [(Q2 + Q4)/(Q1 + Q2 + Q3 + Q4)] × 100 [23].

2.13. Western blot analysis

Total proteins of cells were harvested *via* a radio immunoprecipitation assay buffer (P0013B, Beyotime) with a cocktail, and quantified *via* a bicinchoninic acid assay kit (ST2222-5 g, Beyotime). These proteins were denatured for 10 min (95 °C). Then, the total proteins were run in SDS-PAGE, and the separated proteins were transferred onto polyvinylidene difluoride membranes (Millipore, Bedford, MA, United States). The membranes were exposed to a blocking buffer for 2 h (room temperature) and then incubated with

the different primary antibodies overnight (4 °C): P38 MAPK (1:5000, bf8015, Affinity), p-p38 MAPK (1:1000, af4001, Affinity), and β-tubulin (1:1000, ta-10, ZSGB-BIO). Next, the membranes were washed using tris-buffered saline (TBS) with Tween-20 thrice and cultured with the corresponding secondary antibodies for 4 h (4 °C): goat anti-rabbit IgG (1:6000, zb-2301, ZSGB-BIO), and goat anti-mouse IgG (1:6000, zb-2305, ZSGB-BIO). These membranes were then visualized utilizing the enhanced chemiluminescence reagent (P1020-25, Applygen). The protein band was observed using β-tubulin as the internal reference. Image Lab (National Institutes of Health, Maryland, United States) was used to analyse the gray value of the target band.

2.14. Statistical analysis

Data was analyzed using SPSS 21.0 (IBM Corp., Armonk, NY, United States) and displayed as the mean ± SEM. The GraphPad Prism 8.0 was utilized for data visualization. The level of significance was assessed *via* a one-way analysis of variance (ANOVA) or two-way analysis of variance, with $p < 0.05$. Three independent experiments were repeated with ≥10 cells in each experiment, and every condition was analyzed.

3. Results

3.1. Active compound identification and herbal-component-target network construction

A total of 65 active compounds in YCD were identified [24–28], of which 21 were from *R. astragali*, 18 from *R. rehmanniae*, 13 from *F. gardeniae*, 4 from *H. cistanches*, 3 from *R. aconiti preparata*, 3 from *R. aconiti kusnezoffii preparata*, 1 from *R. astragali* and *F. gardeniae*, 1 from *F. gardeniae* and *H. cistanches*, and 1 from *R. astragali*, *F. gardeniae* and *H. cistanches*, as shown in Table S2. Furthermore, 801 targets were obtained *via* a chemical similarity-based search of these compounds. Using the above data, we constructed an herbal-component-target network consisting of 872 nodes and 3413 edges (Fig. 3).

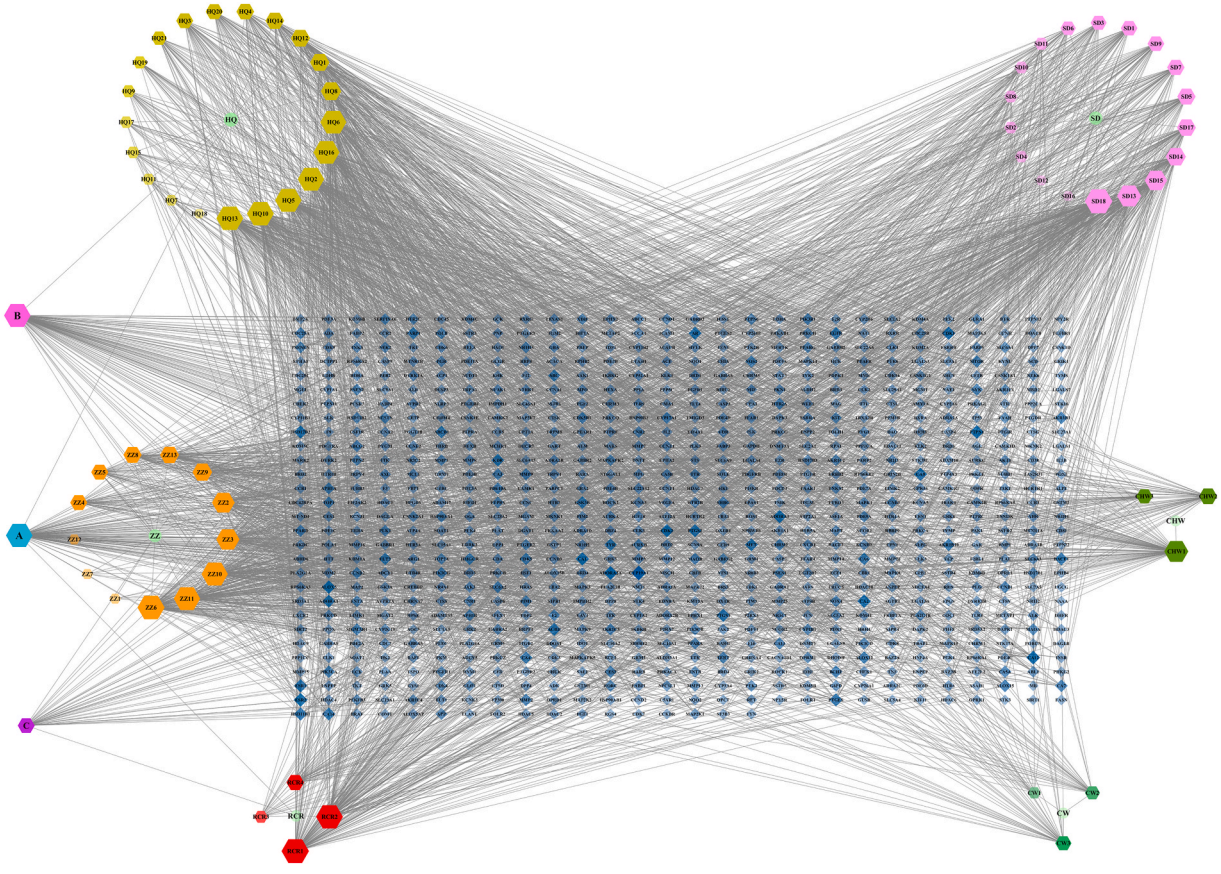

Fig. 3. Herbal-component-target network of YCD. In the figure, a circle represents the herbals; a hexagon represents the active components of herbals; a diamond represents the targets of active components.

3.2. Searching for potential disease targets

We obtained 998 PD-related targets by using the score median as the screening condition (Score ≥12.9283843040467). We compared the YCD to PD-related targets, drew a Venn diagram through Venny2.1, and obtained 172 potential targets shared by YCD and PD (Fig. 4A).

3.3. Establishment of PPI network

We imported 172 anti-PD targets of YCD into the STRING database to generate a network of PPI (Fig. 4B). To get a better visualization and understanding of the PPI network, we downloaded the tsv file of the PPI data. A PPI network was constructed using Cytoscape 3.7.2 consisting of 170 nodes (2 disconnected nodes were deleted) and 3168 edges. Used the medians of the target-related indicators to generate the highly connected sub-network, which comprised 63 nodes and 1284 edges (DC ≥ 31, BC ≥ 0.0018, CC ≥ 0.5339) (Fig. 4C). Through this network, we obtained 63 YCD anti-PD core targets. We speculated that these targets are crucially involved in the claimed YCD anti-PD effect.

3.4. GO enrichment analysis

To further discover the possible biological mechanisms in the regulation of PD by YCD, we performed GO enrichment analysis on 63 core targets. The prominent 20 enriched molecular functions, cell components, and biological processes were screened, the specific analysis results were shown in Fig. 4D–F.

3.5. Selection of the optimized dose and time for rotenone-treated SH-SY5Y cells

We executed a sequence of experiments to verify the reliability of the above bioinformatics analysis. PD cell model was established by rotenone-treated SH-SY5Y cells. The cell viability was measured by CCK-8 assay after different concentrations of rotenone were applied at different time points. The SH cell viability decreased with increasing administration time and rotenone concentration ($p < 0.05$; Fig. 5A). As PD is a chronic progressive disease, it is appropriate to select the lowest concentration for the longest time achieving significant reduction in cell viability for modeling. Therefore, we selected the cells treated with 2 μM rotenone for 48 h for follow-up experiments.

3.6. YCD-medicated serum improved the activity of cells and repaired the morphological damage induced by rotenone

In clinical practice, YCD has a positive effect on delaying the PD's progression, the biological mechanism of which has not been

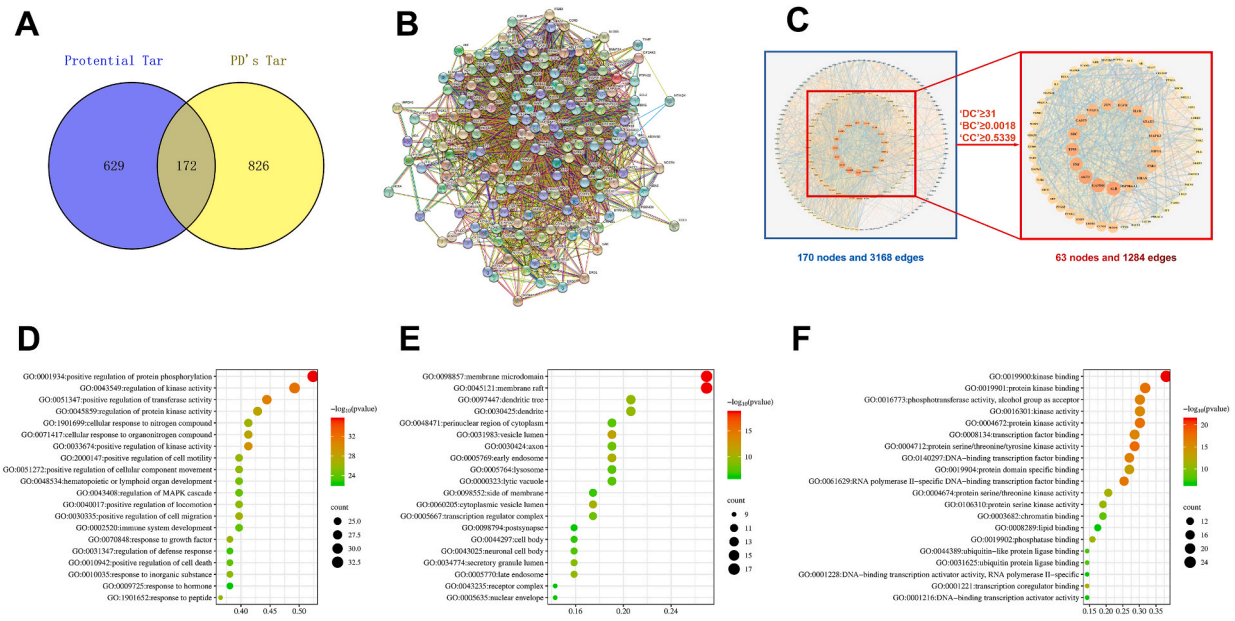

Fig. 4. Screening process of the core YCD anti-PD targets and GO enrichment analysis using the core targets. (**A**) The 172 common potential targets between the YCD-related targets and PD-related targets. (**B**) Generation of PPI network *via* database of STRING. (**C**) Screening strategy diagram of core targets. DC, BC, and CC. (**D-F**) Core anti-PD targets of YCD are used for GO enrichment analysis. (**D**) GO: Biological Processes, (**E**) GO: Cellular Components, and (**F**) GO: Molecular Function.

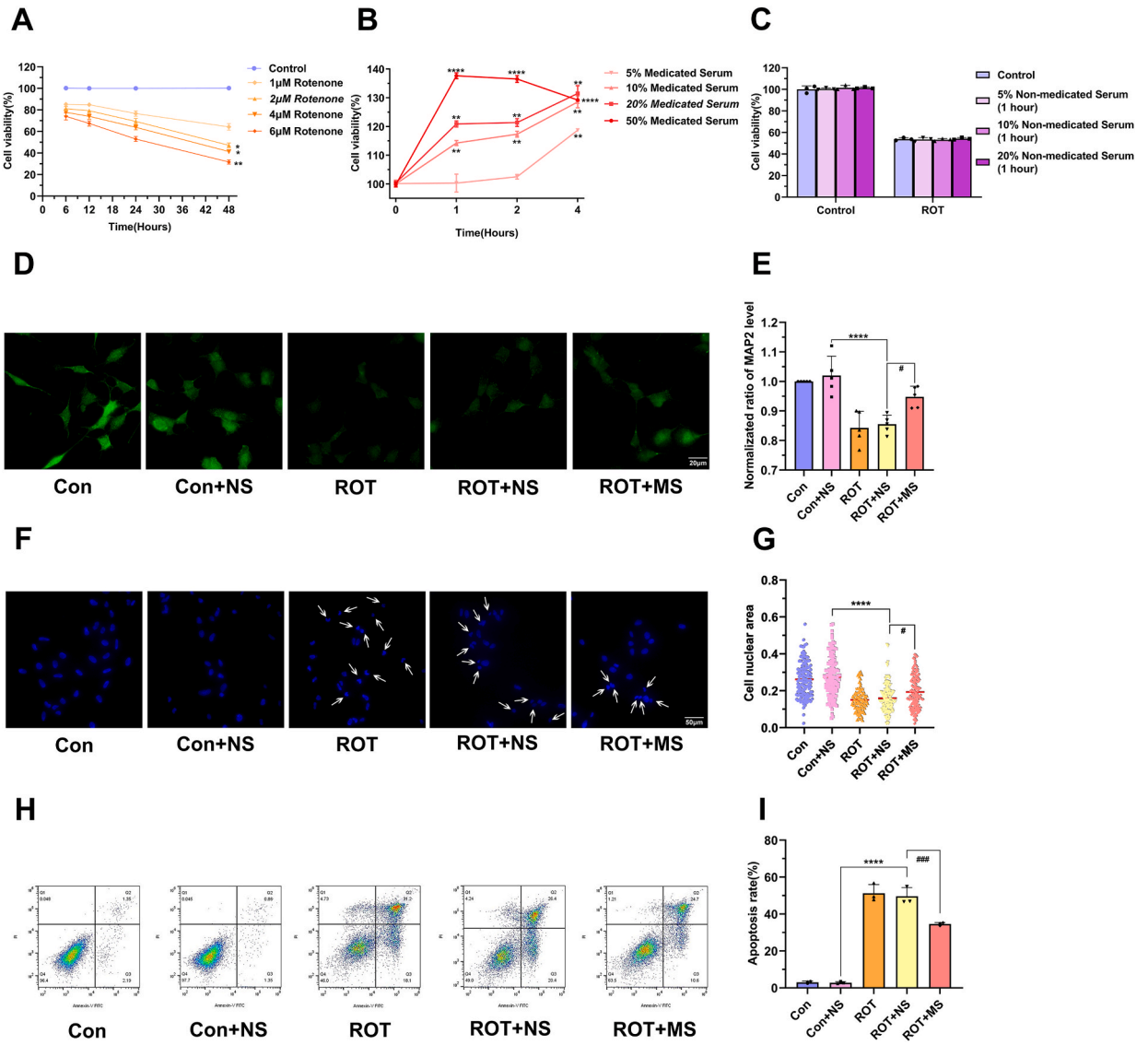

Fig. 5. (**A**) Identify the optimal concentration and induction time for rotenone in SH-SY5Y cells. (**B**) Identify the optimal concentration and treatment duration for YCD-containing serum in SH-SY5Y cells. (**C**) Non-medicated serum (at different concentrations) failed to exhibit any impact on cell viability. (**A-C**) CCK-8 assay was employed to analyse cell survival. (**D, E**) The MAP2 level was detected by immunofluorescence staining. (**F, G**) Cells were tagged with Hoechst 33,342 staining, and the nuclear area was analyzed *via* ImageJ software. (**H, I**) Flow cytometry measured the apoptosis rate in rotenone-treated SH-SY5Y cells. At least three independent experiments were repeated in each experimental verification. Data are illustrated as mean ± SEM. (**A, B**) Comparative analysis of two independent variables *via* two-way ANOVA. $*p < 0.05$, $**p < 0.01$, and $****p < 0.0001$ vs. Control. (**C–I**) Comparative analysis of multiple groups *via* one-way ANOVA, $****p < 0.0001$ vs. Control + non-medicated serum group; $\#p < 0.05$, $\#\#\#p < 0.001$ vs. Rotenone + non-medicated serum group. Con: contral, ROT: rotenone, NS: non-medicated serum, MS: medicated serum.

explored much. Some literature has confirmed that the components extracted from *R. astragali*, *R. rehmanniae*, *H. cistanches* and other herbs have cytoprotective functions and improve the motor function of PD mice model [29–32].

We treated SH cells with YCD-medicated serum diluted with DMEM and calculated the effect of 5 %, 10 %, 20 %, and 50 % YCD-medicated serum at 1, 2, and 4 h on cell viability by CCK-8 assay. We found that treatment with a 5 % concentration of YCD-medicated serum for 1 and 2 h failed to exhibit any impact on cell viability. Cell growth was enhanced by YCD-medicated serum in a concentration dependent pattern, and the growth of cell viability slowed down after 2 h. When the concentration of YCD-medicated serum reached 50 %, the cell viability began to decline after 2 h ($p < 0.05$; Fig. 5B). It is indicated that long-term application of high serum concentration may have a negative effect on cell survival. Then, we pretreated the normal and rotenone-treated cells with 5 %, 10 % and 20 % normal serum for 1 h, and the cell viability of each group was found to be insignificantly different from the control cells ($0.5 < p < 1$; Fig. 5C). Therefore, we selected 20 % serum pretreatment for 1 h as the experimental condition of the treatment group in the

follow-up experiments.

To examine the impact of YCD on morphological disruption of rotenone-treated cells, we used immunofluorescence staining to assess the localizations, levels, and analysis of dendritic protein MAP2 [33] in the cells. As depicted in Fig. 5D and E, the MAP2 level in the model group was remarkably decreased in relation to the control ($p < 0.0001$), while YCD-medicated serum could significantly increase the expression level of MAP2 in rotenone-treated cells ($p < 0.05$). Rotenone-treated cells showed severe damage, with wrinkled nuclei upon Hoechst 33,342 staining. After pretreatment with YCD-medicated serum, the nucleus shrinkage was significantly alleviated ($p < 0.05$; Fig. 5F and G). The above findings indicated that YCD-medicated serum could prevent the reduced cell viability and morphological changes of rotenone-treated SH-SY5Y cells.

3.7. YCD inhibited rotenone-treated apoptosis of SH-SY5Y cells

Rotenone increased the apoptosis of SH cells ($p < 0.0001$), while the YCD pretreatment substantially suppressed the rotenone-induced apoptosis ($p < 0.001$; Fig. 5H and I). Therefore, it is speculated that YCD can prevent the rotenone-induced apoptosis in vitro.

3.8. YCD decreased inflammatory cytokines and oxidative stress in vitro

In comparison with the control, *IL-6, IL-1β*, and *TNF-α* levels were increased in the rotenone-treated cells ($p < 0.01$), YCD-medicated serum reduced significantly these inflammatory mediators ($p < 0.05$; Fig. 6A–C), highlighting that YCD can prevent rotenone-induced cellular inflammation in vitro. Additionally, rotenone increased the ROS level and decreased the SOD activity in SH-SY5Y cells ($p < 0.0001$), while YCD reduced significantly the ROS and increased the SOD activity ($p < 0.01$; Fig. 6D and E). Therefore, YCD pretreatment can exert an antioxidant effect in PD.

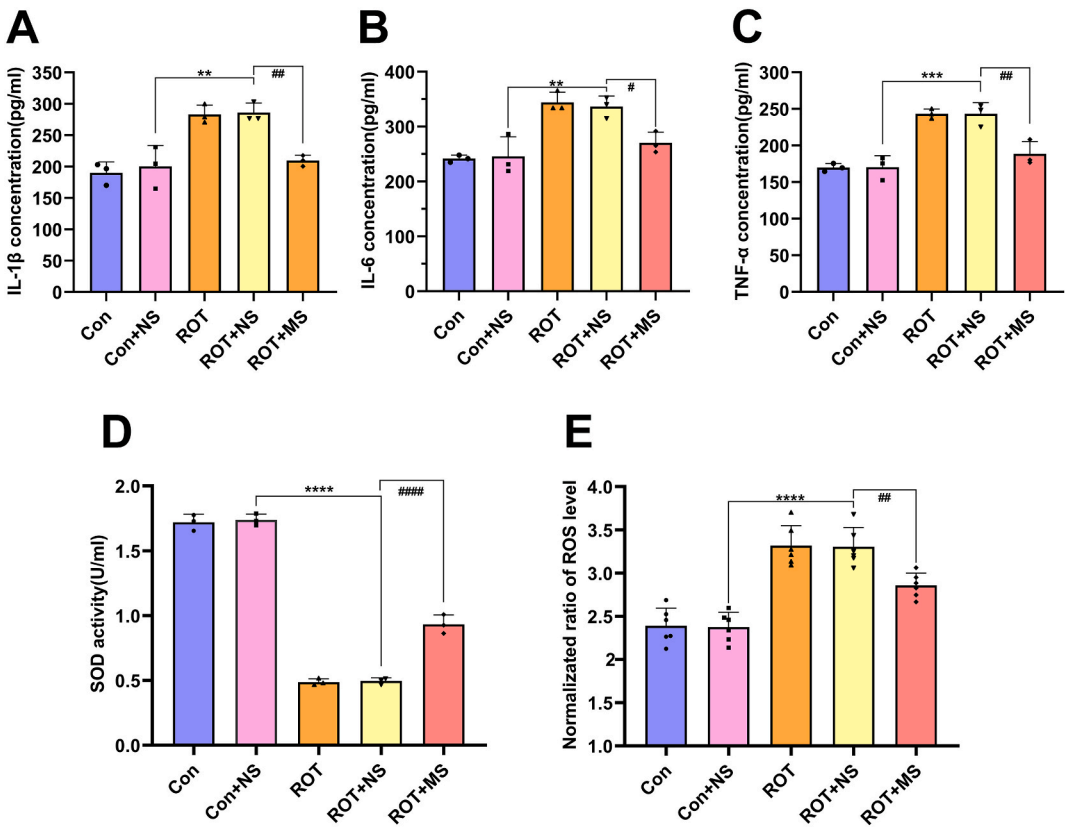

Fig. 6. YCD suppressed the inflammatory cytokines and oxidative stress levels in rotenone-treated SH-SY5Y cells. (**A-C**) The concentrations of *IL-6, IL-1β*, and *TNF-α* in rotenone-treated cells were examined by ELISA. (**D, E**) The level of ROS and activity of *SOD* in rotenone-treated cells were monitored *via* respective kits. At least three independent experiments were repeated in each experimental verification. Data are illustrated as mean ± SEM. Comparative analysis of multiple groups was employed *via* one-way ANOVA, $^{**}p < 0.01$, $^{***}p < 0.001$, $^{****}p < 0.0001$ vs. Control + non-medicated serum group; $\#p < 0.05$, $\#\#p < 0.01$, $\#\#\#\#p < 0.0001$ vs. Rotenone + non-medicated serum group. Con: contral, ROT: rotenone, NS: non-medicated serum, MS: medicated serum.

3.9. KEGG pathway enrichment and target-pathway network

Based on the above experiments, we found that the effect of YCD on the rotenone-induced PD is related to the inhibition of inflammation and apoptosis, but the precise mechanism remains elusive. Thus, we performed KEGG enrichment analysis on the core targets to predict the signal pathway that YCD may participate in. The results indicated that the main regulatory pathways of YCD on PD include lipid and atherosclerosis, MAPK and PI3K-Akt signaling pathways, neurodegenerative and cancer pathways and viral infection (Fig. 7A). We screened the results of KEGG analysis, collected 20 pathways with the highest '-LogP' value and the core targets enriched on the pathways, and constructed the pathway-target network comprising 78 nodes and 421 edges (Fig. 7B).

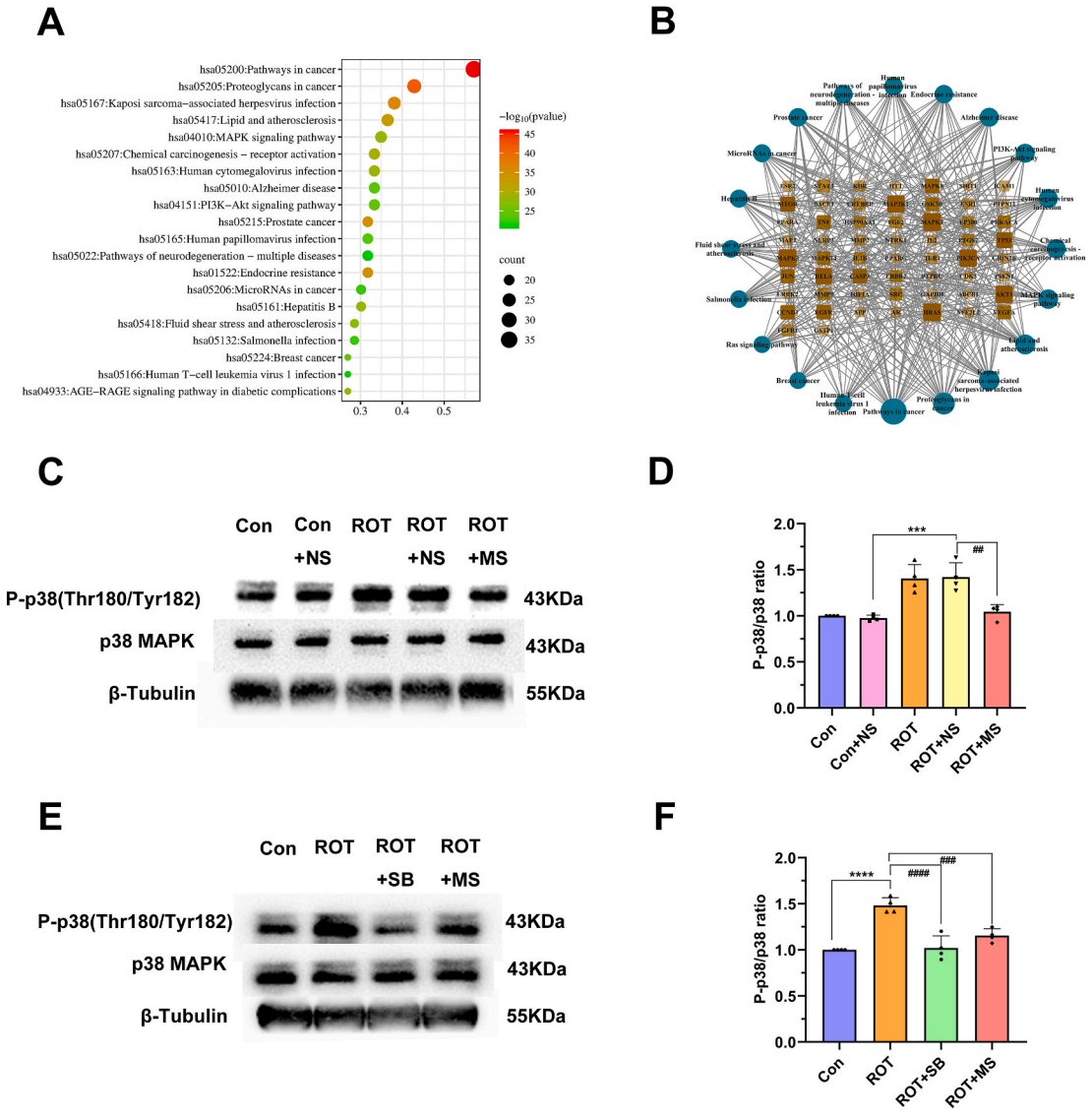

Fig. 7. YCD activated the p38 MAPK pathway in rotenone-treated SH-SY5Y cells. (**A**) Used core anti-PD targets of YCD to perform KEGG pathway enrichment analysis. (**B**) The pathway-target network is involved in the process of YCD anti-PD. In the figure, a circle represents 20 major pathways of YCD anti-PD from KEGG analysis; the square represents the targets enriched from major pathways. (**C–F**) Levels of p38 MAPK and p-p38 were monitored *via* Western blotting. At least three independent experiments were repeated in each experimental verification. Data are illustrated as mean ± SEM. (**C, D**). Comparative analysis within the multiple groups was employed *via* one-way ANOVA, $***p < 0.001$ vs. Control + non-medicated serum group; $\#\#p < 0.01$ vs. Rotenone + non-medicated serum group. The complete blots are shown in Supplementary Fig. 2. (**E, F**) The p38 MAPK pathway inhibitor SB203580 (10 μM) was pre-added to the rotenone-treated (2 μM) cells. Comparative analysis within the multiple groups was employed *via* one-way ANOVA, $****p < 0.0001$ vs. Control group; $\#\#\#p < 0.001$, $\#\#\#\#p < 0.0001$ vs. Rotenone group. The complete blots are shown in Supplementary Fig. 3. Con: contral, ROT: rotenone, NS: non-medicated serum, MS: medicated serum, SB: SB203580.

3.10. Involvement of p38 MAPK signaling in YCD anti-PD effect in vitro

P38 MAPK is involved in neuroinflammation, oxidative stress, and apoptosis in PD. We speculated that YCD might control PD cells *via* the p38 MAPK pathway, thus, we conducted Western blotting to examine the p-p38 and p38 levels. We found that the p-p38 levels were remarkably enhanced ($p < 0.001$) in the model group, while YCD pretreatment remarkably reduced the p-p38 level in rotenone-treated SH-SY5Y cells ($p < 0.01$; Fig. 7C and D). These suggest that YCD exerts protection in rotenone-treated SH cells by reducing the level of p-p38.

3.11. YCD protected rotenone-treated cells by inhibiting the expression of phospho-p38

To validate the involvement of p38 MAPK pathway in YCD protective effect in rotenone-treated SH-SY5Y cells, we blocked the p38 MAPK pathway by pretreating cells with p38 MAPK pathway inhibitor SB203580 (10 μM). In contrast to the model group, the p-p38/p38 ($p < 0.0001$; Fig. 7E and F) and apoptosis rate was substantially reduced in the inhibitor group ($p < 0.0001$; Fig. 8E and F). Immunofluorescence and Hoechst 33,342 staining showed that SB203580 could mitigate the morphological damage of cells caused by rotenone ($p < 0.0001$; Fig. 8A–D). Additionally, the p38 MAPK inhibitor reduced the levels of inflammatory cytokines and ROS but

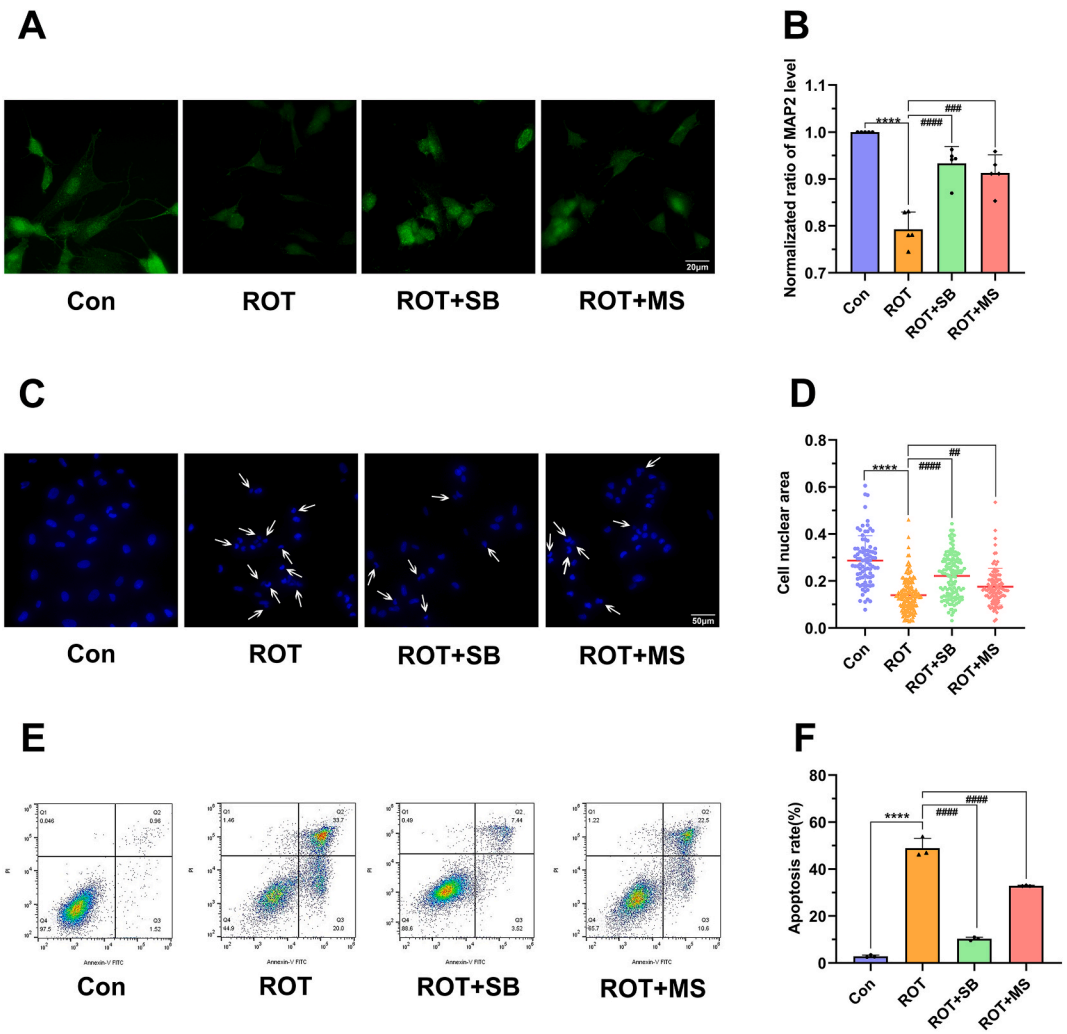

Fig. 8. YCD prevented the apoptosis and morphological changes of rotenone-treated SHSY5Y cells by suppressing the p38 MAPK activation. The p38 MAPK pathway inhibitor SB203580 (10 μM) was pre-added to the rotenone-treated (2 μM) cells. (**A, B**) MAP2 level was detected *via* immunofluorescence staining. (**C, D**) Cells were detected by Hoechst 33,342 staining, and the nuclear area of cells was analyzed by ImageJ software. (**E, F**) The apoptosis rate of rotenone-treated cells was monitored by flow cytometry. At least three independent experiments were repeated in each experimental verification. Data are illustrated as mean ± SEM. Comparative analysis of multiple groups was employed *via* one-way ANOVA, ****$p < 0.0001$ vs. Control group; ##$p < 0.01$, ###$p < 0.001$, ####$p < 0.0001$ vs. Rotenone group. Con: contral, ROT: rotenone, MS: medicated serum, SB: SB203580.

increased SOD activity ($p < 0.01$; Fig. 9A–E). YCD could prevent cellular inflammation, oxidative stress, reduce morphological damage, and apoptosis of rotenone-treated SH-SY5Y cells by suppressing p38 MAPK pathway activation.

4. Discussion

PD exhibits a high prevalence among neurological conditions, positioning it as the second common neurodegenerative disease [34,35]. TCM has gained considerable attention due to its distinctive theoretical system, methodology, and therapeutic effect on PD. Multiple findings have reported the therapeutic utility of TCM in treating PD. Exploring the mechanism of anti-PD effect of TCM can support the use of TCM combined with existing treatment modalities. Nonetheless, "PD" was not mentioned in ancient Chinese medical literature; it can be described as "Tremor syndrome" based on its clinical manifestations. We summarized the PD pathogenesis as wind-cold-dampness blockage and kidney deficiency. Therefore, to better explain the role of YCD, a comprehensive approach combining network pharmacology and experimental validation investigated the possible mechanisms of YCD in PD.

Some studies have reported that *R. astragali, H. cistanches, R. rehmanniae,* and other components in YCD can produce anti-PD effects through different pathways [28,36], thus, we screened the main components and predicted the core targets of YCD. In this study, 65 active compounds in YCD were screened by ADME criteria through TCMSP and Pubmed databases. By using these compounds to predict the targets and compare them with PD targets, we screened 63 core anti-Parkinson targets. Based on the above findings, GO enrichment analysis on a set of 63 core targets revealed significant enrichment in 1420 biological processes, 80 cell components, and 114 molecular functions.

To our knowledge, many studies have reported that various components of *R. astragali* have neuro-protective functions. Astragaloside IV (AS-IV) could reduce cytotoxicity, inhibit inflammation, apoptosis, and oxidative stress, and ameliorate motor deficits in the PD mouse model [23,37,38]. Zhang et al. [39] demonstrated that AS-IV substantially reversed the reduced MPP + -treated cell viability, enhanced intracellular caspase-3 activity, ROS production, and increased *Bax/Bcl-2* ratio. Astraisoflavan and Astragalus polysaccharide (APS) induce neural stem cells (NSCs) differentiation into DA neurons [40]. More recently, Tan et al. [41] have shown that APS exerts an anti-Parkinson effect by stimulating the pathway of PI3K/AKT/mTOR to improve cell viability and autophagy in

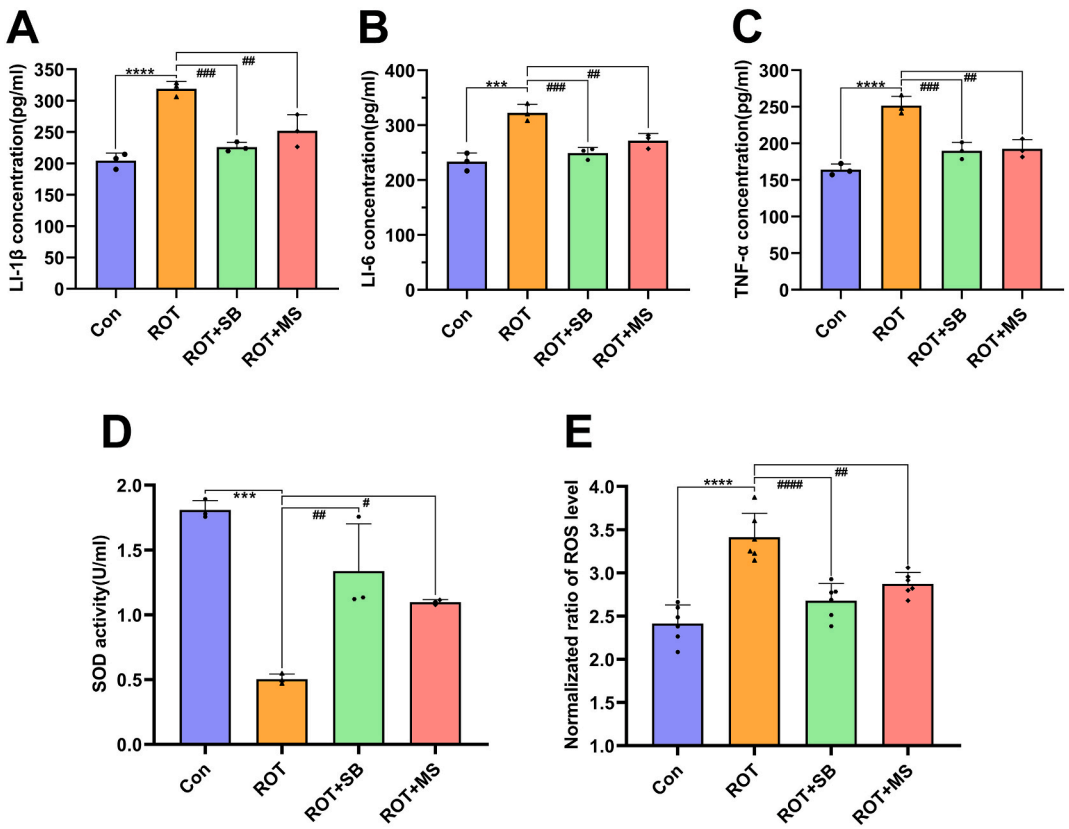

Fig. 9. YCD plays anti-inflammatory and anti-oxidative roles in rotenone-treated SHSY5Y cells by suppressing the activation of the p38 MAPK pathway. The inhibitor SB203580 (10 μM) was pre-added to the rotenone-treated (2 μM) cells. (**A-C**) The concentration of inflammatory mediators in rotenone-treated cells was analyzed by ELISA. (**D, E**) The level of ROS and activity of *SOD* in rotenone-treated cells were monitored *via* respective kits. An experiment was repeated thrice independently. Data are illustrated as mean ± SEM. Comparative analysis within the multiple groups was employed *via* one-way ANOVA, ***$p < 0.001$, ****$p < 0.0001$ vs. Control; #$p < 0.05$, ##$p < 0.01$, ###$p < 0.001$, ####$p < 0.0001$ vs. Rotenone groups. Con: contral, ROT: rotenone, MS: medicated serum, SB: SB203580.

vitro.

Many studies have demonstrated the anti-parkinsonian effect of *H. cistanches* [42]. *H. cistanches* mainly contains phenylethanol glycosides (PhGs), such as echinacoside. Gao et al. [43] have found that echinacoside can improve the survival of DA neurons *in vivo via* stimulating *NLRP3/Caspase-1/IL-1β* signaling pathway. Quercetin enhanced mitochondrial function and exhibited neuroprotective effects on 6-OHDA-induced MN9D cells [44]. Moreover, quercetin increased significantly *SOD* expression, reduced ROS and 4-hydroxy-2-nominal in the SNc, and alleviated behavioral abnormalities in MPTP-induced mice [45]. In conclusion, YCD contains a variety of anti-Parkinson components, which have great potential as an anti-Parkinson medicine.

Rotenone is commonly used to investigate the involvement of dopaminergic cell death in vitro and to test new neuroprotective therapies in PD [46]. Rotenone inhibits mitochondrial complex 1, produces ROS, reduces SOD activity to inhibit ATP synthesis; stimulates microglia and the secretion of *IL-6, IL-1β,* and *TNF-α* [47]; induces apoptosis by activating caspases, p38, and JNK pathways, up-regulating *Bax* and down-regulating *Bcl-2*. In view of this, the rotenone was employed to model PD in SH-SY5Y cell line. The cell viability was reduced to 50 % following treatment with 2 μM rotenone for 48 h. Therefore, we selected the concentration of 2 μM and the time period of 48 h as the experimental conditions for subsequent investigations.

Xu et al. demonstrated that astragaloside IV stimulates the JAK2/STAT3 pathway, thereby improving cell survival and inhibiting oxidative stress, inflammatory response, and apoptosis of 6-OHDA-induced PD models [23]. Echinacoside could significantly improve cell viability, apoptosis, and oxidative stress of 6-OHDA-induced PC12 cells and maintain mitochondrial membrane potential [48]. Consistent with the above studies, our study showed that YCD pretreatment improved cell viability, repaired morphological damage, reduced apoptosis, and reduced inflammation and oxidative stress levels in rotenone-treated SH-SY5Y cells.

Neuroinflammation and oxidative stress are crucially involved in the onset of chronic neurodegenerative diseases, such as PD, Amyotrophic lateral sclerosis, and Alzheimer's disease. They are regarded as the main causes of DA neuron death in the pathological course of PD [49]. Therefore, many TCMs with anti-oxidative properties have received much attention to prevent and cure PD progression [50]. Activated microglia secretes inflammatory cytokines, causing inflammation. Dysfunction of complex I within the electron transport chain (ETC) of the mitochondria produces ROS, resulting in oxidative stress [51,52]. In this study, we detected the inflammatory response in cells, which alleviated with YCD pretreatment. Similarly, YCD pretreatment increased *SOD* activity and reduced ROS level. Consequently, YCD exerted anti-inflammatory and anti-oxidative effects in vitro PD model.

The p38 MAPK pathway, being a canonical signaling cascade, in the pathogenesis and advancement of several diseases [53]. The stimulation of p38 MAPK is a key factor in PD, and is strongly linked to cell proliferation and cell death [54]. In this study, rotenone promoted the p-p38 expression, which was considerably alleviated by YCD, indicating that YCD may prevent the expression of downstream inflammatory cytokines and ROS *via* suppressing the p38 MAPK stimulation. Moreover, we added SB203580, the p38 MAPK inhibitor, to the reaction system, which substantially suppressed the levels of inflammatory mediators, ROS, and p-p38 MAPK in rotenone-treated SH-SY5Y cells, increased SOD activity, decreased apoptosis rate, and improved morphological changes. Based on the results, we found that SB203580 may have better preventive effects on inflammation and apoptosis than YCD in SH-SY5Y cell PD model. A variety of inhibitors have been used in experimental studies and their suitability for humans remains to be determined. However, YCD has been used as a clinical drug, and its effects on PD might not limited to preventing inflammation and apoptosis, which needs more experiments and clinical trials to verify.

Collectively, our findings indicated that YCD treatment may reduce rotenone-treated inflammation, oxidative stress, and apoptosis by suppressing the p38 MAPK in vitro PD model. Further investigation is needed to elucidate the mechanisms of anti-PD effect of YCD.

5. Conclusions

The current study employed network pharmacology and in vitro experiments to elucidate YCD's biological process in PD's therapeutic management. We identified 63 anti-PD targets in YCD, which were highly correlated to signaling pathways of MAPK, PI3K-Akt and neurodegenerative pathways. YCD reduced cell inflammation and apoptosis by inhibiting p38 MAPK pathway to achieve anti-PD effect.

Data availability statement

Data included in article/supplementary material/referenced are presented in the article.

Ethics statement

The animal study was reviewed and approved (202106A024) by Animal Ethics Committee of Nanjing University of Chinese Medicine (Nanjing, China).

Funding resources

This research project was supported by the Natural Science Foundation of Jiangsu Province of China (BK20230447); Jiangsu Traditional Chinese Medicine Science and Technology Development Project (QN202202; QN202201); Luo LinXiu Teacher Development Fund Project (LLX202312; LLX202206); Special Research Project of Nantong Health and Family Planning Commission (QN2023022).

CRediT authorship contribution statement

Dong Di: Writing – original draft, Visualization, Validation. **Chencheng Zhang:** Visualization, Resources, Project administration, Methodology, Investigation. **Suping Sun:** Validation. **Ke Pei:** Visualization, Supervision. **Renjun Gu:** Visualization, Supervision. **Yan Sun:** Visualization, Supervision. **Shihan Zhou:** Supervision. **Yanqing Wang:** Validation. **Xinyi Chen:** Validation. **Shan Jiang:** Validation. **Haoxin Wu:** Supervision. **Boran Zhu:** Resources, Methodology, Funding acquisition, Conceptualization. **Xu Xu:** Supervision, Resources, Funding acquisition.

Declaration of competing interest

The authors declare that they have no known competing financial interests or personal relationships that could have appeared to influence the work reported in this paper.

Acknowledgements

We would like to thank Jiangsu Huasino Pharmaceutical Technology Co., Ltd (Jiangsu, China) for providing Sprague Dawley rats, and the Science and Technology Center of Nanjing University of Chinese Medicine (Jiangsu, China) for assistance with High Performance Liquid Chromatography analysis.

Appendix A. Supplementary data

Supplementary data to this article can be found online at https://doi.org/10.1016/j.heliyon.2024.e34823.

Abbreviations

PD (Parkinson's disease)
YCD (Yishen chuchan decoction)
NP (network pharmacology)
TCM (traditional Chinese medicine)
TCMSP (Traditional Chinese Medicine System Pharmacology)
PPI (protein-protein interaction)
SD (Sprague-Dawley)
CCK (Cell Counting Kit)-8
MAP2 (microtubule associated protein 2)
p38 MAPK (mitogen-activated protein kinase)
p-p38 (phospho-p38)
IL (Interleukin)-1β
IL (Interleukin)-6
TNF (Tumor Necrosis Factor)-α
MAO-B (monoamine oxidase B)
DR (dopamine receptor)
OB (bioavailability)
DL (drug-likeness)
DC (degree centrality)
CC (closeness centrality)
BC (betweenness centrality)
HRP (Horseradish peroxidase)
FITC (Fluorescein isothiocyanate)
R. Astragali (radix astragali)
F. Gardeniae (fructus gardeniae)
H. Cistanches (herba cistanches)
R. Rehmanniae (radix rehmanniae)
R. aconiti preparata (radix aconiti preparata)
R. aconiti kusnezoffii preparata (radix aconiti kusnezoffii preparata)
NS (normal saline)
LAS X (Leica Application Suite X)
ELISA (Enzyme-Linked Immunosorbent Assay)
ROS (reactive oxygen species)
SOD (superoxide dismutase)
PI (propidium iodide)
V-FITC (V-fluorescein isothiocyanate)

TBS	(tris-buffered saline)
ANOVA	(analysis of variance)
α-syn	(α-synuclein)
DA neurons	(dopaminergic neurons)
SNc	(substantia nigra pars compacta)
6-OHDA	(6-hydroxydopamine)
MPTP	(1-methyl-4-phenyl-1,2,3,6-tetrahydropyridine)
COX-2	(cyclooxygenase-2)
AS-IV	(Astragaloside IV)
APS	(Astragalus polysaccharide)
NSCs	(neural stem cells)
PhGs	(phenylethanol glycosides)
ETC	(electron transport chain)

References

[1] O.B. Tysnes, A. Storstein, Epidemiology of Parkinson's disease, J. Neural. Transm. 124 (8) (2017 Aug) 901–905.
[2] P.J. Garcia-Ruiz, K.R. Chaudhuri, P. Martinez-Martin, Non-motor symptoms of Parkinson's disease a review from the past, J. Neurol. Sci. 338 (1–2) (2014 Jan) 30–33.
[3] D.K. Simon, C.M. Tanner, P. Brundin, Parkinson disease epidemiology, pathology, genetics, and pathophysiology, Clin. Geriatr. Med. 36 (1) (2020 Feb) 1–12.
[4] R.B. Postuma, D. Berg, M. Stern, et al., MDS clinical diagnostic criteria for Parkinson's disease, Mov. Disord. 30 (12) (2015 Oct) 1591–1601.
[5] F.C. Church, Treatment options for motor and non-motor symptoms of Parkinson's disease, Biomolecules 11 (4) (2021 Apr 20) 612.
[6] A.E. Lang, A.J. Espay, Disease modification in Parkinson's disease: current approaches, challenges, and future considerations, Mov. Disord. 33 (5) (2018 May) 660–677.
[7] J.A. Obeso, M. Stamelou, C.G. Goetz, et al., Past, present, and future of Parkinson's disease: a special essay on the 200 th Anniversary of the Shaking Palsy, Mov. Disord. 32 (9) (2017 Sep) 1264–1310.
[8] Y.Y. Liu, L.H. Yu, J. Zhang, et al., Network pharmacology-based and molecular docking-based analysis of suanzaoren decoction for the treatment of Parkinson's disease with sleep disorder, BioMed Res. Int. 2021 (2021 Oct 8) 1752570.
[9] W. Zhuang, M. Cai, W. Li, et al., Polyphenols from Toona sinensiss seeds alleviate neuroinflammation induced by 6-hydroxydopamine through suppressing p38 MAPK signaling pathway in a rat model of Parkinson's disease, Neurochem. Res. 45 (9) (2020 Sep) 2052–2064.
[10] C. Gai, W.D. Feng, T.Y. Qiang, et al., Da-bu-yin-wan and qian-zheng-san ameliorate mitochondrial dynamics in the Parkinson's disease cell model induced by MPP, Front. Pharmacol. 10 (2019 Apr 24) 372.
[11] H.J. Ma, C. Gai, Y. Chai, et al., Bu-yin-qian-zheng formula ameliorates MPP+-Induced mitochondrial dysfunction in Parkinson's disease via parkin, Front. Pharmacol. 11 (2020 Dec 18) 577017.
[12] B.Y. Zeng, Effect and mechanism of Chinese herbal medicine on Parkinson's disease, Int. Rev. Neurobiol. 135 (2017) 57–76.
[13] J. He, W. Zhong, M. Zhang, et al., P38 mitogen-activated protein kinase and Parkinson's disease, Transl. Neurosci. 9 (2018 Nov 12) 147–153.
[14] J. Ru, P. Li, J. Wang, et al., TCMSP: a database of systems pharmacology for drug discovery from herbal medicines, J. Cheminf. 6 (2014 Apr 16) 13.
[15] X. Xu, W. Zhang, C. Huang, et al., A novel chemometric method for the prediction of human oral bioavailability, Int. J. Mol. Sci. 13 (6) (2012) 6964–6982.
[16] C.Y. Jia, J.Y. Li, G.F. Hao, et al., A drug-likeness toolbox facilitates ADMET study in drug discovery, Drug Discov. Today 25 (1) (2020 Jan) 248–258.
[17] A. Daina, O. Michielin, V. Zoete, SwissADME: a free web tool to evaluate pharmacokinetics, drug-likeness and medicinal chemistry friendliness of small molecules, Sci. Rep. 7 (2017 Mar 3) 42717.
[18] A. Daina, O. Michielin, V. Zoete, SwissTargetPrediction: updated data and new features for efficient prediction of protein targets of small molecules, Nucleic Acids Res. 47 (W1) (2019 Jul 2) W357–W364.
[19] P. Shannon, A. Markiel, O. Ozier, et al., Cytoscape: a software environment for integrated models of biomolecular interaction networks, Genome Res. 13 (11) (2003 Nov) 2498–2504.
[20] G. Stelzer, N. Rosen, I. Plaschkes, et al., The GeneCards suite: from gene data mining to disease genome sequence analyses, Curr Protoc Bioinfo 54 (1.30.1–1.30.33) (2016 Jun 20).
[21] A.B. Nair, S. Jacob, A simple practice guide for dose conversion between animals and human, J. Basic Clin. Pharm. 7 (2) (2016 Mar) 27–31.
[22] V. Sharma, J.H. McNeill, To scale or not to scale: the principles of dose extrapolation, Br. J. Pharmacol. 157 (6) (2009 Jul) 907–921.
[23] Z. Xu, D. Yang, X. Huang, et al., Astragaloside IV protects 6-hydroxydopamine-induced SH-SY5Y cell model of Parkinson's disease via activating the JAK2/STAT3 pathway, Front. Neurosci. 15 (2021 Mar 23) 631501.
[24] P. Liu, H. Zhao, Y. Luo, Anti-aging implications of Astragalus membranaceus (huangqi): a well-known Chinese tonic, Aging Dis 8 (6) (2017 Dec 1) 868–886.
[25] K.K. Auyeung, Q.B. Han, J.K. Ko, Astragalus membranaceus: a review of its protection against inflammation and gastrointestinal cancers, Am. J. Chin. Med. 44 (1) (2016) 1–22.
[26] W. Xiao, S. Li, S. Wang, C.T. Ho, Chemistry and bioactivity of Gardenia jasminoides, J. Food Drug Anal. 25 (1) (2017 Jan) 43–61.
[27] Y. Fu, B. Liu, J. Liu, et al., Geniposide, from Gardenia jasminoides Ellis, inhibits the inflammatory response in the primary mouse macrophages and mouse models, Int. Immunopharm. 14 (4) (2012 Dec) 792–798.
[28] Y. Zhou, K. Yang, D. Zhang, et al., Metabolite accumulation and metabolic network in developing roots of Rehmannia glutinosa reveals its root developmental mechanism and quality, Sci. Rep. 8 (1) (2018 Sep 20) 14127.
[29] B.Y. Zeng, Effect and mechanism of Chinese herbal medicine on Parkinson's disease, Int. Rev. Neurobiol. 135 (2017) 57–76.
[30] H. Gao, L. Dou, L. Shan, et al., Proliferation and committed differentiation into dopamine neurons of neural stem cells induced by the active ingredients of radix astragali, Neuroreport 29 (7) (2018 May 2) 577–582.
[31] J.Q. Liang, L. Wang, J.C. He, et al., Verbascoside promotes the regeneration of tyrosine hydroxylase-immunoreactive neurons in the substantia nigra, Neural Regen Res 11 (1) (2016 Jan) 101–106.
[32] C. Gu, X. Yang, L. Huang, Cistanches herba: a neuropharmacology review, Front. Pharmacol. 7 (2016 Sep 20) 289.
[33] A. Caceres, G. Banker, O. Steward, L. Binder, M. Payne, MAP2 is localized to the dendrites of hippocampal neurons which develop in culture, Brain Res. 315 (1984) 314–318.
[34] S.Y. Lim, A.H. Tan, A. Ahmad-Annuar, et al., Parkinson's disease in the western pacific region, Lancet Neurol. 18 (9) (2019 Sep) 865–879.
[35] J. Liu, W. Liu, R. Li, et al., Mitophagy in Parkinson's disease: from pathogenesis to treatment, Cells 8 (7) (2019 Jul 12) 712.
[36] P. Chen, J. Zhang, C. Wang, et al., The pathogenesis and treatment mechanism of Parkinson's disease from the perspective of traditional Chinese medicine, Phytomedicine 100 (2022 Jun) 154044.

[37] H. Li, Y. Zhang, J. Min, et al., Astragaloside IV attenuates orbital inflammation in Graves' orbitopathy through suppression of autophagy, Inflamm. Res. 67 (2) (2018 Feb) 117–127.
[38] C. Yang, Y. Mo, E. Xu, et al., Astragaloside IV ameliorates motor deficits and dopaminergic neuron degeneration via inhibiting neuroinflammation and oxidative stress in a Parkinson's disease mouse model, Int. Immunopharm. 75 (2019 Oct) 105651.
[39] Z.G. Zhang, L. Wu, J.L. Wang, et al., Astragaloside IV prevents MPP⁺-induced SH-SY5Y cell death via the inhibition of Bax-mediated pathways and ROS production, Mol. Cell. Biochem. 364 (1–2) (2012 May) 209–216.
[40] H. Gao, L. Dou, L. Shan, et al., Proliferation and committed differentiation into dopamine neurons of neural stem cells induced by the active ingredients of radix astragali, Neuroreport 29 (7) (2018 May 2) 577–582.
[41] Y. Tan, L. Yin, Z. Sun, et al., Astragalus polysaccharide exerts anti-Parkinson via activating the PI3K/AKT/mTOR pathway to increase cellular autophagy level in vitro, Int. J. Biol. Macromol. 153 (2020 Jun 15) 349–356.
[42] H. Lei, X. Wang, Y. Zhang, et al., Herba cistanche (rou cong rong): a review of its phytochemistry and pharmacology, Chem. Pharm. Bull. (Tokyo) 68 (8) (2020) 694–712.
[43] M.R. Gao, M. Wang, Y.Y. Jia, et al., Echinacoside protects dopaminergic neurons by inhibiting NLRP3/Caspase-1/IL-1β signaling pathway in MPTP-induced Parkinson's disease model, Brain Res. Bull. 164 (2020 Nov) 55–64.
[44] M. Ay, J. Luo, M. Langley, et al., Molecular mechanisms underlying protective effects of quercetin against mitochondrial dysfunction and progressive dopaminergic neurodegeneration in cell culture and MitoPark transgenic mouse models of Parkinson's Disease, J. Neurochem. 141 (5) (2017 Jun) 766–782.
[45] T. Benameur, R. Soleti, C. Porro, The potential neuroprotective role of free and encapsulated quercetin mediated by miRNA against neurological diseases, Nutrients 13 (4) (2021 Apr 16) 1318.
[46] K. Radad, M. Al-Shraim, A. Al-Emam, et al., Rotenone: from modelling to implication in Parkinson's disease, Folia Neuropathol. 57 (4) (2019) 317–326.
[47] O. Yoshino, Y. Osuga, Y. Hirota, et al., Endometrial stromal cells undergoing decidualization down-regulate their properties to produce proinflammatory cytokines in response to interleukin-1 beta via reduced p38 mitogen-activated protein kinase phosphorylation, J. Clin. Endocrinol. Metab. 88 (5) (2003 May) 2236–2241.
[48] Y.H. Wang, Z.H. Xuan, S. Tian, et al., Echinacoside protects against 6-hydroxydopamine-induced mitochondrial dysfunction and inflammatory responses in PC12 cells via reducing ROS production, Evid Based Complement Alternat Med 2015 (2015) 189239.
[49] R. Yin, J. Xue, Y. Tan, et al., The positive role and mechanism of herbal medicine in Parkinson's disease, Oxid. Med. Cell. Longev. 2021 (2021 Sep 3) 9923331.
[50] F. Muhammad, Y. Liu, Y. Zhou, et al., Antioxidative role of traditional Chinese medicine in Parkinson's disease, J. Ethnopharmacol. 285 (2022 Mar 1) 114821.
[51] P.R. Angelova, Sources and triggers of oxidative damage in neurodegeneration, Free Radic. Biol. Med. 173 (2021 Sep) 52–63.
[52] A. N Kolodkin, R.P. Sharma, A.M. Colangelo, et al., ROS networks: designs, aging, Parkinson's disease and precision therapies, NPJ Syst Biol Appl 6 (1) (2020 Oct 26) 34.
[53] C. Falcicchia, F. Tozzi, O. Arancio, et al., Involvement of p38 MAPK in synaptic function and dysfunction, Int. J. Mol. Sci. 21 (16) (2020 Aug 6) 5624.
[54] J. He, W. Zhong, M. Zhang, et al., P38 mitogen-activated protein kinase and Parkinson's disease, Transl. Neurosci. 9 (2018 Nov 12) 147–153.